Drilling of Fiber-Reinforced Plastics - Tool Modeling and Defect Prediction

Athulan Vijayaraghavan

January 23, 2006

Abstract

Fiber reinforced polymer (FRP) composites have been steadily replacing metals as choice engineering materials for various applications. Although FRPs can be manufactured to near-net shape, post processing operations such as machining are required to create some features (such as holes). In order to drill holes efficiently with the least waste and defects, it is essential to understand the machining behavior of FRPs. As FRPs are multiphase materials with complex load-response behavior, there is a need to turn to analytical and numerical approaches to fully understand the machining process. This report discusses a model to analytically estimate the edge defect in drilled FRP laminates. The model predicts that increasing drilling thrust force causes greater delamination and thus, greater edge defects. The report also discusses a tool which can create automated 3D CAD drill models based on geometric as well as manufacturing parameters. This tool is a required component of numerical/FE-models of FRP drilling. The tool outputs the drill in a variety of solid geometry formats which can then be meshed and used in different FE analysis packages.

Contents

Chapter 1

Introduction

Fiber reinforced polymer (FRP) composites have been steadily replacing metals as choice engineering materials for various applications. This has especially been the case in the aerospace industry where FRPs are used in the construction of aircraft structural members. Although FRPs can be manufactured to near-net shape, post processing operations such as machining are not entirely avoidable to create some features, especially holes. Indeed, drilling is arguably the most common post-processing operation performed on FRP composites.

In order to drill holes efficiently with the least waste and defects, it is essential to understand the machining behavior of FRPs. Traditional machining research has relied extensively on using experiments to understand machining behavior, but as materials get more complex obtaining results from experiments can become very cumbersome. Hence there is a need to turn to alternate methods in lieu of experimental techniques and this is where we find analytical and numerical modeling techniques useful. Let us first take a look at what FRP composites are and why such a modeling approach is preferred.

1.1 What are FRP Composites?

A composite material can be defined as "a multiphase material with chemically dissimilar phases separated by a distinct interphase" [1]. Composite materials are inherently anisotropic in the macroscale due to the multiple phases (in many cases, the phases themselves are anisotropic) and it is possible to design the materials with controlled anisotropy. This makes composites very useful in applications where specific engineering properties are needed in specific material orientations.

Although composites can be made of several phases, in the most general case the constituents can be modeled as a matrix phase surrounding a dispersed reinforcement phase.

3

Usually, the reinforcement provides load bearing properties while the matrix ensures efficient load distribution. Based on the type of reinforcement, composites can be classified as particle-reinforced and fiber-reinforced. Fiber-reinforced composites may be either have continuous, aligned fibers or discontinuous, short fibers as reinforcement. Some of these types are shown in Figure 1.1. This report deals exclusively with continuous fiber-reinforced polymer-matrix composites.
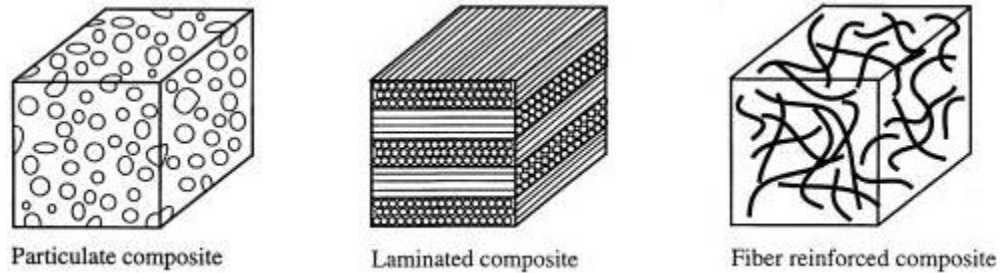
Figure 1.1: Some Composite Material Types (Adapted from [2])

Fiber reinforced composites are usually used in the forms of laminates. A laminate is made by bonding two or more lamina together. Lamina usually are made of parallel fibers set in a polymer matrix at some constant volume fraction. The laminate is assembled with the individual lamina at different fiber orientations. Figure 1.2 shows the individual laminae (which are at different angular orientations) as well as a fully assembled FRP composite. The load-response behavior and engineering properties of the laminate are determined by both the fiber orientations in the lamina and the order in which they are assembled together in the laminate.

Figure 1.2: Laminated Fiber-reinforced Composite (Adapted from [3])

1.2 FRPs and the Aerospace Industry

Multilayer materials (or stackups) are used extensively in the construction of aerospace structural members. They provide increased strength-weight ratios compared to traditional structural material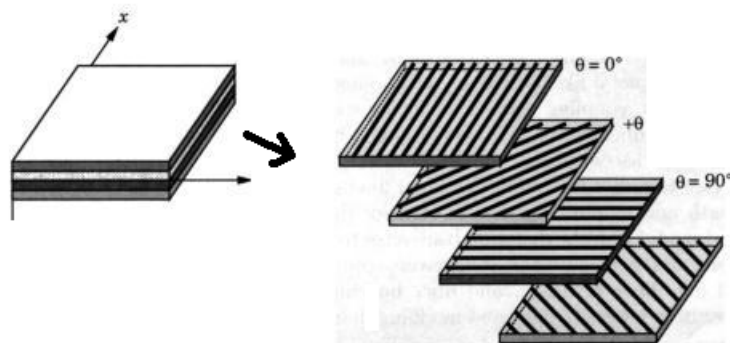. Also, the different layers provide a wide range of functionality that increases the utility of the structural member. Composite materials are being used increasingly as constituents of these stackups. Typical aerospace panel stackups include: CFRP/CFRP (CFRP - Carbon Fiber Reinforced Polymers), CFRP/Titanium, CFRP/Titanium/CFRP, and CFRP/Aluminum.

The principal machining operation performed on aerospace structures is drilling. These structures are usually assembled and drilled in one operation during which interface burrs are formed and debris from machining is also lodged between the layers. The aim is to control the formation of the interface burrs and accumulation of the debris. The need in industry is to be able to drill through these layers in one operation without need for any rework (i.e. without having to disassemble and clean the parts before fastening). Currently, deburring operations account for about 30% of the total manufacturing cost [4].

The major aircraft manufacturers, Boeing and Airbus, are shifting from traditional aerospace alloys to composite stackups for use in their new aircraft designs (Figure 1.3). Airbus achieved significant weight savings due to switching from Aluminum trusses to composite trusses, also leading to better fuel economy and a lower operating cost. Airbus extensively uses GLARE or Glass Reinforced Aluminum which is a proprietary material developed in conjunction with Delft University (Figure 1.4). Boeing is developing composites which can be used in the construction of the airplane fuselage. Figure 1.5 shows the use of a drilled metal-composite stackup in a Boeing 777. The metal is Titanium and the composite is Carbon Fiber Reinforced Polymer (CFRP).

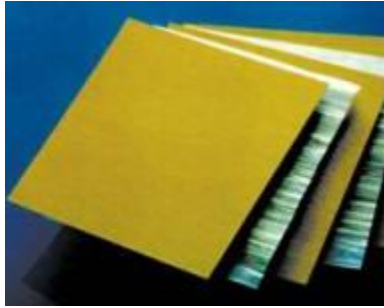Figure 1.3: Airbus A380 and Boeing 787 [5, 6]
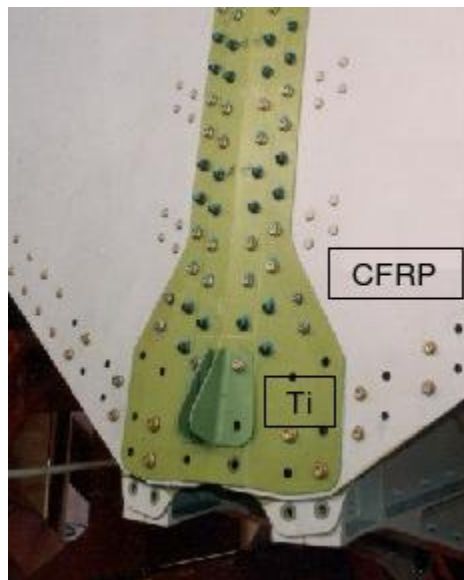
Figure 1.4: GLARE - Glass Reinforced Aluminum [7]

Figure 1.5: Tail section of Boeing 777 with Ti-CFRP-Ti stackup [4]

1.3   Need for a Modeling Approach

While experimental methods and empirical models have been the mainstay of machining research, the useful information provided from experimental techniques is limited by the quality of the experiments and the capability of the measuring experiment. Transient and dynamic phenomenon such as strain-rates, temperature at the cutting zone, stress-fields cannot be easily estimated from experiments. Moreover, experiments can be cumbersome to setup and it may take a lot of time to perform data analysis on experimental results. Given these shortcomings of experimental methods, it makes sense to turn to analytical and numerical methods for understanding material machining behavior.

Analytical models can be used to estimate the relations between manufacturing behavior and material properties. Hence, information from analytical models can be used for material selection and for relating process phenomena with specific materials. Moreover, analytical models places a connection between observable phenomenon (such as defects) and physical phenomenon (stress/strain).

Numerical methods are a natural extension of analytical formulations. Numerical methods such as the Finite Element method, use elements from analytical models as constitutive relationships to develop detailed models of machining. These methods can provide detailed information on the process on facets such as stress-strain behavior, temperature variations, crack propagation etc., For this information to be accurate, it is important to setup the appropriate constitutive relationships which can be very labor intensive. But with computers getting faster and our requirements from analysis increases to better optimize processes, numerical methods are becoming effective tools to study manufacturing processes.

Ultimately, the effectiveness of analytical and numerical model can be verified only if they conform with experimental results. But this given, analytical and numerical models offer capable replacements for experimental results by offering rapid and detailed results, respectively.

1.4   Report Objectives

This report presents an analytical model to estimate the edge defect during the drilling of FRP composites. It also discusses the development of a software tool to model a drill suitable for use in numerical machining simulations. These two projects form a part of the "bigger picture" which aims to develop a fully-featured numerical model of FRP drilling. The first topic presented - the analytical model - estimates the defects that occur around the hole

edge when drilling through an FRP. The second topic presented - the drill modeler software tool - is an easy way to create accurate, digital 3D cutting tool geometry which can be then applied in a numerical simulations.

The next section looks into more detail at FRP composites and proposes a framework of features that numerical FRP machining simulations have to capture for accurate modeling.

Chapter 2

Challenges in Modeling FRP Machining

The unique properties of FRP composites have to be explicitly taken into consideration when they are modeled. As much of the machining models have focused on metals and metal-like materials, it is useful to consider the issues that have to be addressed when modeling FRP composites. As a detailed discussion of analytical models in machining is beyond the scope of this report[1], let us first take a look at past-work in finite-element modeling of metal machining. Following this, the differences in properties between metals and FRPs are discussed followed by some of the issues finite-element and other methods have to address when modeling FRP machining.

2.1   Finite Element Modeling

Significant work has been done in modeling metal cutting using the finite element method. The earliest models such as those by Komvopolous & Erpenbeck [10] and Strenkowski & Carroll [11] defined a parting line to denote the region of chip separation. Huang & Black [12] discussed several chip separation criteria classifying them broadly as geometric and physical, and suggest the best criteria to apply for accurate simulations. More sophisticated chip separation criteria employ continuous re-meshing techniques like the one proposed by Marusich and Ortiz [13]. Klocke et al [14] used a plastic failure criterion to model chip separation.

Specifically focusing on modeling burr formation, Park [15] presented a Lagrangian finite

---

[1]The reader is directed to Shaw [8] and Trent & Wright [9] who discuss machining models extensively in their texts on this subject.

element model for burr formation in orthogonal cutting. A parting line method was used to model material separation and chip formation. He also studied the effect of using a backup material on burr formation. Min et al [16] developed a FE drilling model that showed burr formation at the exit surface. The model simulated the formation of a crown and uniform burr as a function of the feed rate and shows that a uniform burr is formed at lower feeds and a crown burr is formed at higher feeds. The failure criterion was based on the equivalent plastic strain in the discrete elements. When the plastic strain reached a certain limit in an element, it was removed from the simulation space. Choi [17] adapted this model and simulated gap and interfacial burr formation when drilling two SS304L layers (Figure 2.1).
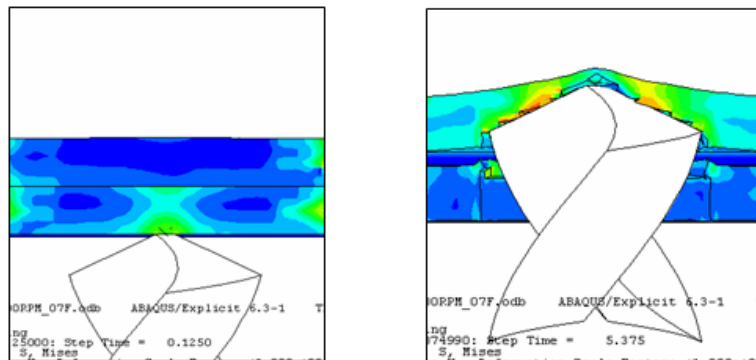

Figure 2.1: Inter-layered Burr in Drilling of Two Sheets of SS 304L [17]

Most metal cutting simulations use Lagrangian descriptions of the deforming material where the mesh is fixed to the workpiece, experiencing deformation along with the work-piece. Lagrangian models encounter difficulties due to the large material deformations of metal cutting which results in severe mesh distortion. This can be overcome by using mesh adaptivity controls and continuous re-meshing. Specific criteria also have to be defined to model chip separation. A notable exception to this is the work of Hsu [18] who used a combined Lagrangian and Eulerian modeling technique. In Eulerian techniques the mesh is fixed to space and not to the deforming body.

2.2 FRP Modeling

The principal difference between metals and composite materials is that the former can be modeled as homogeneous while the latter cannot. Clear distinctions have to be made between the fiber and the matrix as they vary widely in properties. Hence, for accurate modeling, the constitution of the composite has to be explicitly known. This information

may either be deterministic or stochastic. Composite materials are anisotropic which makes their machining quite different from that of metals. Also, as their behavior can change dramatically with temperature, heating effects also have to be observed. This is especially true in the case of composites with polymer matrices; the high temperatures of machining can result in phase change in the fiber resulting in significant changes in the machining behavior [19]. Generalized observations on chip formation cannot be made for composite machining as the chip morphology depends on the orientation and properties of the matrix and the fiber. Chip formation can also be because of both fracture and shear. In order to better model composite materials, it is useful to look at some of their distinct properties which have to be captured in machining models.

2.2.1 Failure Modes

It is significantly harder to predict failures in composites when compared to metals. Failure is often of a random nature, and hence statistical tools may be needed for accurate prediction. Also, there are several failure modes and all of their effects need to be considered. There are five significant failure modes for FRPs (Fiber Reinforced Polymers) - longitudinal compression, longitudinal tension, transverse compression, transverse tension and shear failure. These failure modes have to be considered for both the fiber and the matrix [20]. There are two broad types of failure criteria for these materials - limit and interactive. Limit criteria considers each of these modes as independent of each other and sets failure to occur when at least one of these individual criteria are fulfilled. Interactive criteria, on the other hand, consider the interaction of these different modes with one another and take into account all of their effects in predicting composite failure. Clearly, interactive criteria are more sophisticated and accurate in predicting composite failure. Soden et al [21] and Hinton et al [22] prepared a comprehensive comparison of various FRP failure theories. The authors apply the various theories in 14 test cases of biaxial loading to determine which theories offer the best predictive results.

Delamination is also a significant failure mode in laminated composites. Delamination failure is determined by the interlaminar fracture energy and is caused by out-of-plane stresses. The complex stress-strain response of laminated composites may result in even planar forces causing out-of-plane stresses which may result in delamination.

2.2.2 Failure Growth and Cracks

FRP composites exhibit crack formation in the form of micro-cracks. Cracks in composites do not cause catastrophic failure as in metals but usually cause local failure. Also, as mentioned, out-of-plane stresses may cause delamination cracks between the layers. Crack propagation is also very different from that in metals as composites are not homogeneous. Cracks propagate differently depending on the strength of the matrix-fiber bond. If the matrix-fiber bond is very strong, then cracks originating in the matrix extend across the fiber. If the bond is weak, the crack may extend in separate paths across the matrix and the fiber.

2.2.3 Stress Concentration Effects

The free end planes of the composite laminates also have to be specifically considered for failure during the simulation. Stress concentrations are seen in these end planes and may cause failure in the form of cracks and delamination. Stress concentration is also seen in the edges of other features when axial loads are applied to laminates. This is especially pertinent in the modeling of drilling through a laminate where another feature (eg. a hole) is already present in the laminate. It is also possible for different regions of a composite laminate to have different pre-stresses (this is common when laminates are used as structural members for Aerospace applications [4][2]).

2.2.4 Thermal Effects

FRP composite materials generally have poorer conductive properties when compared to metals. This leads to increased temperature during machining Also FRPs may have pre-stresses from the thermal contraction of fibers as they get cooled during manufacture.

2.3 Review of FRP Machining

There has been considerable work in studying the machining of FRP composites. Komanduri [23] identified that the fiber orientation is the major influencer of the cutting properties of FRP. Bhatnagar et al [24] presented observations on chip formation and cutting forces in the orthogonal cutting of unidirectional CFRP laminates. For a detailed discussion of different

---

[2]Stress concentrations may be present both as an unfavorable vestige of the manufacturing process and by design for better strength.

work in this field, the reader is directed to Gordon and Hillery's [25] review of cutting of composite materials.

Arola et al [26] used a Finite Element model to simulate chip formation in orthogonal cutting of FRPs using a dual-mode failure method. Failure was simulated as primary fracture, consisting of fiber failure and secondary fracture, consisting of matrix failure. The fiber orientation angle was assumed as the shear plane angle and the primary fracture plane was defined using experimental results. Principal cutting forces predicted using this method agreed with experimental results, though the thrust force predictions did not concur with experimental results. As this method uses a very rudimentary material model, accurate chip and burr morphologies could not be simulated.

Mahdi and Zhang [27] modeled the machining of a 3D cell of an FRP composite consisting of a fiber and its surrounding matrix. An adaptive meshing technique based on a shear stress criterion was used to handle excessive distortion and element separation was achieved using a maximum shear stress criterion. They also presented a 2D model of machining an FRP composite predicting the cutting force [28]. The material is modeled in a homogeneous anisotropic manner and the model shows some concurrence with experimental results. The obvious limitation with this approach is that composites cannot be modeled as homogeneous material. Moreover, this approach cannot predict chip or burr formation.

2.4 Framework for FE Modeling of FRP Machining

From the above treatment, we can see that in order to provide accurate results, FE models have to fully capture the complex thermo-mechanical response of FRP composites during machining. Based on the above discussion, the following framework for FE models is proposed such that this complex behavior can be accurately simulated.

1. **Model Type -** Lagrangian models are very popular in application to machining problems. As much work has been done using Lagrangian formulations, it will be apt to use them for FRP models as well. Moreover, FRPs do not suffer excessive plastic deformation unlike metals, hence mesh deformation will not be as much an issue in the case of FRP machining as it is for metal-machining.

2. **Adaptive Meshing -** Adaptive meshing controls may not be required in the case of just FRP machining as FRPs do not suffer very large deformation. The model will need to have a mesh which has high local densities in regions where material removal/failure

is expected. This region usually corresponds to the path of the tool as well as regions of high stress concentration.

3. **Thermal Effects -** A thermo-mechanically coupled model must be employed which is capable of accommodating a wide range of thermal properties within the FRP. The model must also take into account the thermal behavior at the interphase.

4. **Material Failure -** Material separation and failure can modeled using one of the many failure models described above or using other criteria such as a parting line. Material separation is critical for modeling chip formation. An element that can model failure has to be used in defining the workpiece. FRPs also exhibit micro-crack formation and delamination cracks so the model should be able to simulate the onset and propagation of these cracks. Failure may also occur at arbitrary places and not just in the region of the tool (as it is common in machining) so the FE-model should not "look" for failure just in the region of the tool but in the entire workpiece.

5. **Contact -** The model should be capable of full thermo-mechanical contact between the different phases present in the FRP as well as between other materials that may form the workpiece (this is especially true in the case of stacked drilling).

6. **Tool Modeling -** The tool should be modeled as a dynamic object which suffers both stress and thermal effects. Tool wear models should be incorporated to consider the effect of wear on chip and burr formation. Multiple wear models may need to be accommodated in the case of stackup drilling as FRPs and metals cause tool wear by different mechanisms.

Chapter 3

Quantifying Edge Defects in FRP Drilling

This section of the report examines the imprecisions that are observed at the hole edge when drilling fiber reinforced polymers and presents an analytical model to quantitatively estimate them. The model predicts the defects by considering the incomplete cutting of the fiber in parts of the laminate that have already delaminated.

Existing work on machining FRPs, specifically looking at drilling and drilling defects is first discussed. This is followed by a detailed discussion of the formulation of the model. Some results from the model, specifically looking at the relationship between process parameters and drill defects is discussed. Qualitative comparisons are also made between the model's predictions and experimental observations. The last sections looks in detail at various techniques that can be used to accurately quantify these defects using contact and non-contact measurement techniques.

3.1   Literature Review

As a general discussion of FRP machining has been presented in Chapter 2, let us look at work specific to drilling defects. Hocheng and Dharan [29] presented the first model that attempted to predict the occurrence of delamination during drilling of fiber reinforced composites. The model used Linear Elastic Fracture Mechanics (LEFM) to calculate the thrust force at which the critical strain energy release rate for delamination is reached. Two modes of delamination failure were identified, push-out during drill exit and peel-up during drill entry. During push-out delamination, the uncut-thickness decreases as the drill is fed through the material and at a critical point the drilling thrust force exceeds the inter-

laminar bond strength resulting in delamination. Peel-up delamination occurs in the same mechanism; the cutting action introducing a peeling force upwards forcing the layers to delaminate. According to the model, the critical force is estimated as:

$$F_A^* = \pi \left[\frac{8 G_{IC} E h^3}{3(1 - \nu^2)} \right]^{\frac{1}{2}}$$

(3.1)

where,

F_A^* Critical thrust force for delamination

G_{IC} Interlaminar fracture energy

E Elastic Modulus

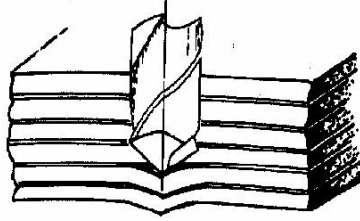ν Poisson's Ratio

h Ply thickness

Figure 3.1: Pushout Delamination [29]

Jain and Yang [30] revisited the work of Hocheng and Dharan and took into account anisotropy effects in determining the critical thrust force for delamination of the laminate, though continuing to use the LEFM assumption. Due to the anisotropic assumption, the model predicted an elliptical delaminated zone as opposed to a circular zone. According to this model, the critical force is estimated as:

$$F_A^* = 3\pi \left[\frac{D_{22}}{D_{11}} \right]^{\frac{1}{4}} \sqrt{2 G_{IC} D_C^*}$$

(3.2)

$$D_C^* = 2 D_{11} + \frac{2(D_{11} + 2 D_{66})}{3} \sqrt{\frac{D_{11}}{D_{22}}}$$

(3.3)

where, $D_{11} = \frac{E_{11} h^3}{12(1 - \nu_{12} \nu_{21})}$, $D_{22} = \frac{E_{22} h^3}{12(1 - \nu_{12} \nu_{21})}$, $D_{12} = \frac{\nu_{12} E_{22} h^3}{12(1 - \nu_{12} \nu_{21})}$ and $D_{66} = \frac{G_{66} h^3}{12}$.

Lachaud et al [31] also used an LEFM-based method to estimate the critical thrust force, but modeled the drilling forces as a distributed load instead of a point load. This model also took into account material anisotropy. The critical force is:

16

$$F_A^* = 8\pi \left[\frac{G_{IC}D}{\left(\frac{1}{3}\right) - \left(\frac{D'}{8D}\right)} \right]^{\frac{1}{2}} \tag{3.4}$$

$$D' = \left(\frac{1}{8}\right)(3D_{11} + 2D_{12} + 4D_{66} + 3D_{22}) \tag{3.5}$$

Zhang et al [32] presented a detailed study which looked at two major kinds of defects during drilling of FRPs - spalling and fuzzing. Spalling refers to delamination damage and fuzzing refers to the uncut fibers around the hole. An empirical relationship between the size of the delamination zone and various process parameters was developed, with fuzzing damage discussed on qualitative terms. Characteristics of an exit defect as described in their work is shown in Figure 3.2.
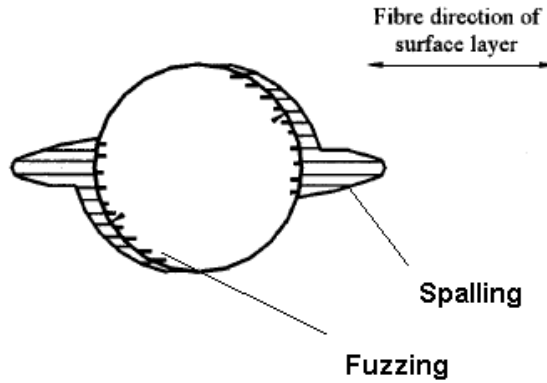

Figure 3.2: Edge Defect Schematic, adapted from Zhang et al [32]

Bhatnagar et al [33] tried to quantify the drilling-induced damage in GFRP composite laminates. They measured the defect size by dye-injection and correlated the damage to process parameters as well as drill geometry parameters. Their experiments showed that the drilling induced damage was lesser for a 8-faceted drill point and a "Jodrill" compared to a standard 4-faceted drill point.

3.2 Model Description

The model estimates edge-defects by looking at the lamina that have delaminated during drilling. We know that the thrust force from drilling causes delamination in the FRP's lamina. As drilling continues after delamination, the delaminated lamina suffer bending from the thrust forces. When the lamina get cut by the drill they are in a deformed state due to the thrust force. Assuming elastic deformation behavior, it is possible to characterize

the deformed state of the fibers as a function of the thrust force. The model does not take into account the deformation behavior of the composite matrix and entirely ignores its effect in causing the edge defect. This is a valid first-order assumption as the matrix is usually a soft, pliable plastic that does not remain uncut unlike the hard, brittle fibers. It is also hard to distinguish between the matrix and the fiber and since the model assumes isotropic plate behavior, the matrix's effect is taken into consideration implicitly.

Once the drilling stops, the thrust force is removed from the fibers and as the deformation is elastic, they revert to the undeformed state. When the length of fiber that has been removed in the deformed state is calculated, it is apparent that lesser fiber than required by the hole dimensions has been removed. This difference in required length removed and actual length removed manifests as the edge defect. A schematic of this phenomenon is shown in Figure 3.3.
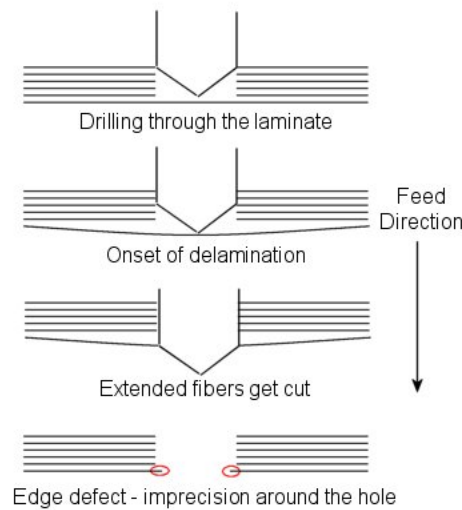

Figure 3.3: Edge Defect Schematic

It is to be noted that this model is a *mechanistic* model and not a *material removal* model. The model assumes that the drill cuts cleanly and is fully efficient in material removal. The model characterizes the edge defect only using the mechanistic effects of cutting, such as the thrust force and the mechanical properties of the laminate, such as modulus and Poisson's ratio.

3.3 Analytical Formulation

To obtain a quantitative measure of the edge imprecision, the delaminated composite lami-
nate is considered as a clamped plate under the load of a concentrated force. The Hocheng-
Dharan model was modified by Won [34] to predict in which lamina delamination occurs for
a given thrust force. The critical force for delamination to occur in the nth lamina (where
the bottom-most lamina is the 1st lamina) is given by:

$$F_A^* = \frac{8G_{IC}E(nh)^3}{3(1-\nu^2)} \tag{3.6}$$

It is obvious that as n increases the effective thickness of the delaminating layer increases,
thereby increasing the critical thrust force necessary for delamination. The critical thrust
force is also a function of lamina material properties and increases with increasing elastic
modulus. Keeping with the assumptions of the Hocheng-Dharan model, the composite is
modeled as an isotropic and homogeneous circular plate. The size of the plate is determined
by the extent of delamination (the delaminated zone). This load causes the bending of the
laminate. The displacement $w(r)$ due to bending (as a function of the distance from the
center, r) is given as [35]:

$$w(r) = \frac{F_A(a^2 - r^2)}{16\pi D} \tag{3.7}$$

where, a is the size of the delaminated zone and D is the rigidity modulus and is:

$$D = \frac{Eh^3}{12(1-\nu^2)}$$

Using this relationship, the deformed length of the fiber before cutting as well as the
deformed length of the fiber that is cut can be calculated. As we have assumed elastic
deformation, the length of the remaining fiber after cutting and after the deformation load
has been removed can also be estimated. Using the theoretical length of fiber remaining
after perfect cutting, the edge defect can be calculated.

The normalized edge defect, r_b is calculated for each fiber across the hole as follows:

L - Length of one fiber from center-plane of hole to delaminated zone edge

l_m - Length of fiber to be removed by drill

l_d - Length of deformed fiber (this is calculated from the arc-length formula[1]):

$$l_d = \int_0^L (1 + w'(r)^2) dr \tag{3.8}$$

l_c - Length of deformed fiber that gets cut:

$$l_c = \int_0^{l_m} (1 + w'(r)^2) dr \tag{3.9}$$

l_{rd} - Deformed fiber length after cut:

$$l_{rd} = l_d - l_c \tag{3.10}$$

l_r - Length of fiber after load is removed. Homogeneous elastic loading is assumed for the deformation response of the fiber.

$$l_r = l_{rd} \frac{L}{l_d} \tag{3.11}$$

l_t - Length of theoretical remaining fiber length assuming perfect drilling

$$l_t = L - l_m \tag{3.12}$$

l_b - Length of defect in fiber:

$$l_b = l_r - l_t \tag{3.13}$$

r_b - Normalized defect:

$$r_b = \frac{l_b}{l_m} \tag{3.14}$$

These calculations are illustrated in Figure 3.4.

3.4 Application of the Model

3.4.1 Hole Geometry

Using the model, the geometry of defects around a hole drilled through an FRP can be seen in Figure 3.5. It can be seen that the defects are maximum for the fiber sections that are longest across the hole and that the resultant hole is elliptical and not circular as intended. Lachaud

---

[1]This is the standard formula from calculus that is used to find the length of an arc. Length of $f(x)$ from x_1 to x_2 is $\int_{x_1}^{x_2} (1 + f'(x)^2) dx$
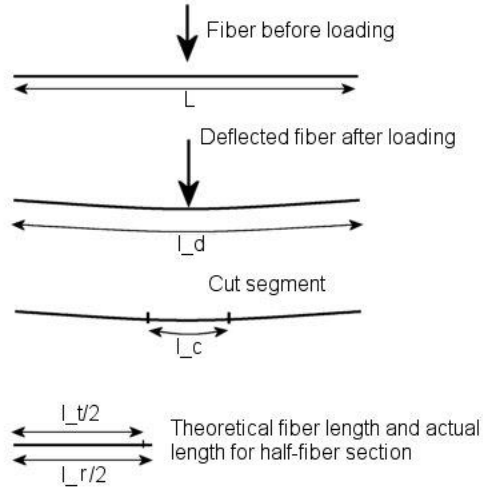
Figure 3.4: Calculating the edge defect

et al [31] also discuss observing this kind of a defect during drilling. This corresponds to the case of using a 5mm drill with a High Modulus CFRP (Carbon-Fiber Reinforced Polymer) workpiece, assuming a constant delaminated zone size (diameter) of 2.5r (where r is the drill radius).

3.4.2   Effect of Thrust Force

It can be seen from the model that the relative imprecision around the hole increases with the thrust force. This is studied in Figure 3.6, where the relative imprecision r_b is plotted as a function of varying thrust force and drill radii. The material is HM-CFRP and a constant delamination zone size of $2.5r$ is assumed.

From the figure it can be observed that the relative imprecision increases monotonically with increasing thrust force, and becoming "flat" beyond a point. The relative imprecision also increases with increasing hole radii, implying that the absolute imprecision will increase even more rapidly with increasing hole radii. It can also be noted from the figure that until the critical delaminating thrust force is reached, the model predicts that no defects will occur.
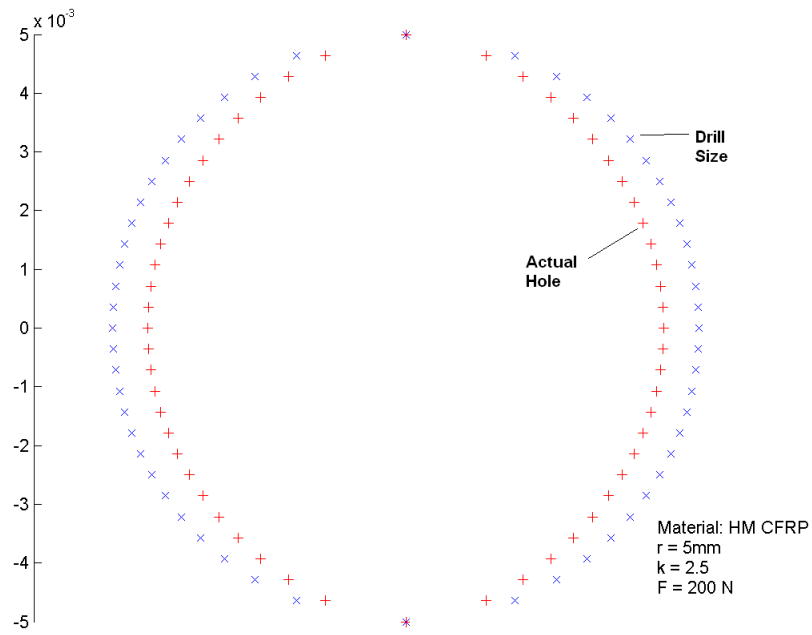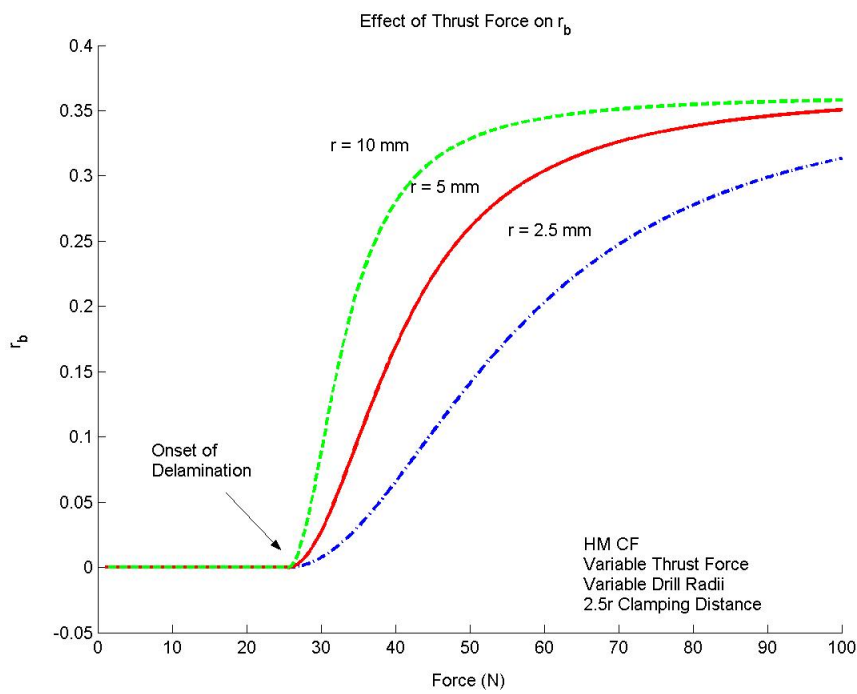
Figure 3.5: Hole Geometry Prediction

Figure 3.6: Effect of Force and 'r'

3.4.3 Effect of Process Parameters

From a practical point of view, it is important to study the effect of drilling parameters like feed on the extent of edge imprecision. Several studies have established the relationship on feed and thrust force in drilling. Shaw [36] proposed the following relationship between feed and thrust force:

$$F_A = k_1(fd)^{1-a} + k_2 d \tag{3.15}$$

where F_A is the axial cutting force, f is the feed in $\frac{mm}{s}$ and d is the diameter of the drill in mm. a, K_1 and K_2 are experimentally determined constants. Won and Dharan [34] used Shaw's equations to model the relationship between feed and thrust force for drilling High Modulus CFRP with a Carbide drill. The thrust force was measured for experiments with varying drill sizes and the feed. From this data, the coefficients of Shaw's equations were calculated for this material, and they are as follows: $a = 0.4011$, $K_1 = 31.31$, $K_2 = -.0571$.

Using this data, the effect of feed on the defect size can be studied. Figure 3.7 shows the effect of increasing feed on r_b for three different drill radii. As feed increases, so does the thrust force and hence, r_b. Thus a relationship between process parameters and defect size can be realized, and this information can be used to set limits on process parameters in order to minimize defects. The material used is a high-strength carbon fiber-polymer (HS-CFRP) and a constant delamination zone size of $2.5r$ is assumed (this is the same material that Won [34] used). The plot shows that delamination (and hence, defect formation) occurs earlier if a larger drill is used. This is a direct result of Shaw's equation, which shows that F_A is larger for a larger d, given the same f.

3.4.4 Effect of the Delaminated Zone

From the model it can be seen that the uncut fiber length depends on the size of the delaminated zone. Hence it is important to accurately characterize the size of the delaminated zone in order to have an effective model. Figure 3.8 shows the variation of the edge defect with changing force for two constant delaminated zone sizes (where the zone size is kr). It can be seen that the defects markedly increase with increasing delaminated zone size.

Existing work ([29], [30], [31]) characterizing the delamination of FRPs during drilling employ Linear Elastic Fracture Mechanics (LEFM). While LEFM successfully predicts the critical thrust force for the onset of edge defect initiation, it is not adequate for predicting the length of the delaminated zone. LEFM prescribes that when the critical strain energy release rate is achieved in the material during drilling, the delaminating crack propagates
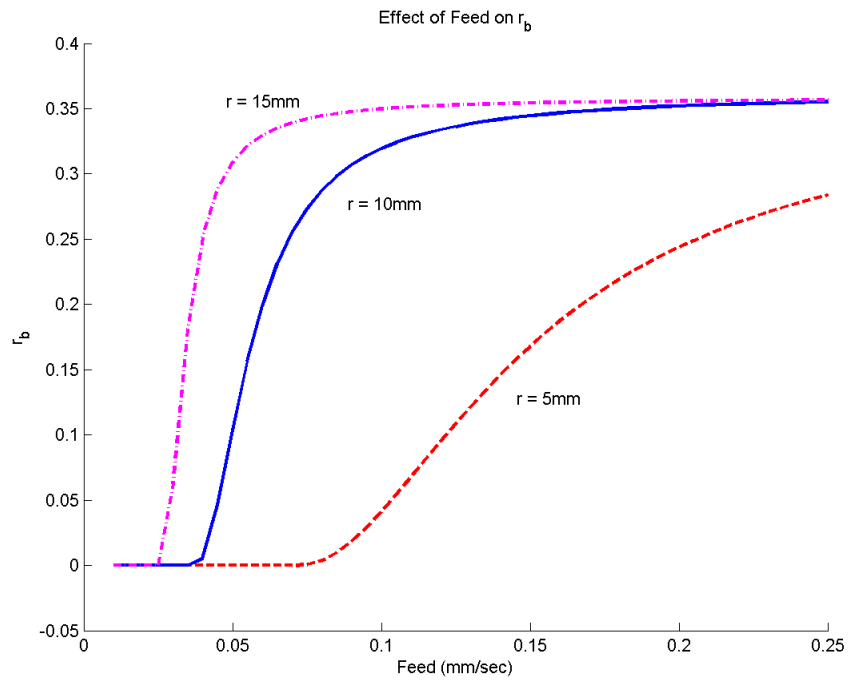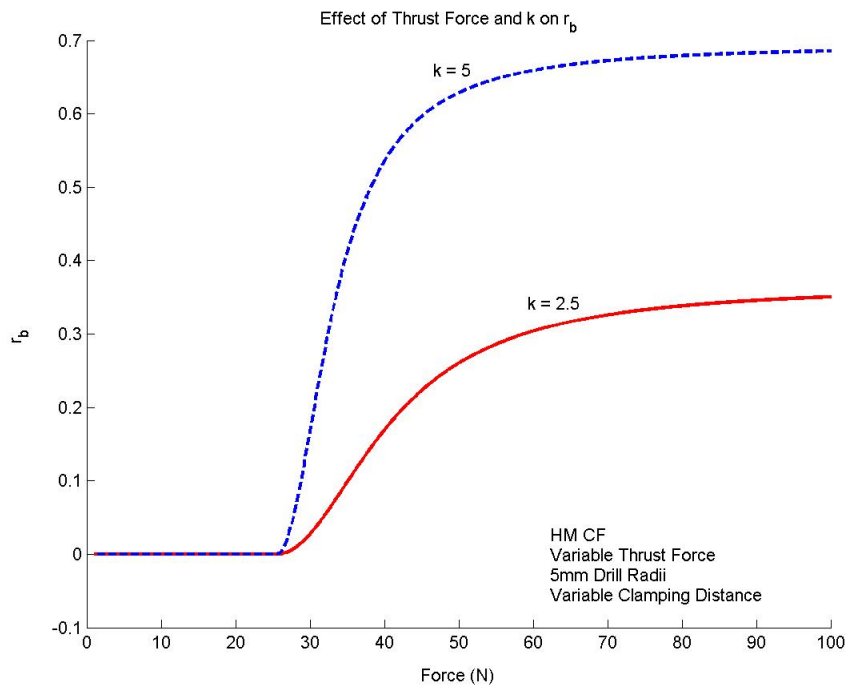
Figure 3.7: Effect of Feed and 'r'

Figure 3.8: Effect of Delaminated Zone Size

24

indefinitely resulting in an infinite delaminated zone. From experimental observations it is quite clear that this is not the case and that the delaminated zone is limited to only a small region immediately around the hole and not to the entire workpiece that is being machined.

Experimental observations by Hocheng [37] and Zhang et al [32] show that the size of the delaminated zone is related to the thrust force during drilling. Hocheng [37] measured the size of the delamination zone for drilling through different FRP composites including Graphite/Epoxy and Glass/Epoxy and used a linear-fit to explain the relationship between the thrust force and the delaminated zone size.

Zhang et al [32] performed experiments to estimate the delaminated zone size as a function of process parameters. Several parameters including the feed, speed and drill radii were varied and an empirical relationship was formulated using a regression fit of the experimental results. The relationship is as follows (l - delaminated zone size, D - diameter, v - feed speed, n - cutting speed, F - thrust force, E - fiber modulus, a, b, k - dimensionless curve-fit parameters):

$$l = k \left(\frac{nD}{\nu} \right)^a \left(\frac{F}{ED^2} \right)^b \tag{3.16}$$

Zhang et al [32] also measured the size of the delaminated zone as a function of thrust forces for drilling through CFRP using a 5.5mm drill. This is shown in Figure 3.9. Using this information, the edge defect can be calculated as a function of both thrust force and delaminated zone size, which is shown in Figure 3.10.
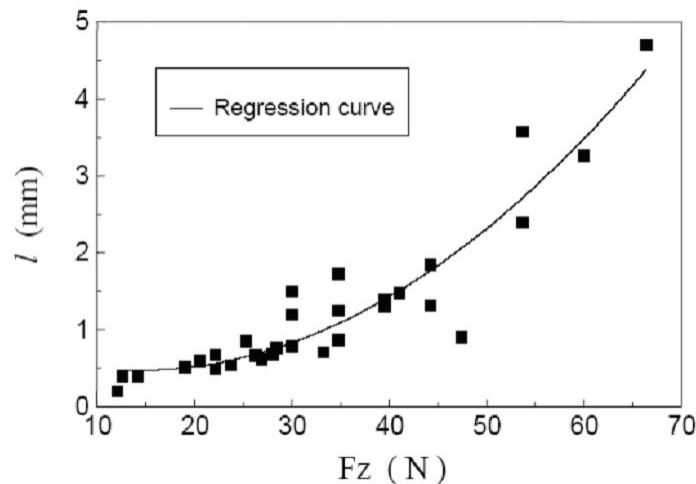

Figure 3.9: Delaminated Zone Variation with Thrust Force [32]

The results indicate that the increase of the edge defect is sharp when the delaminated
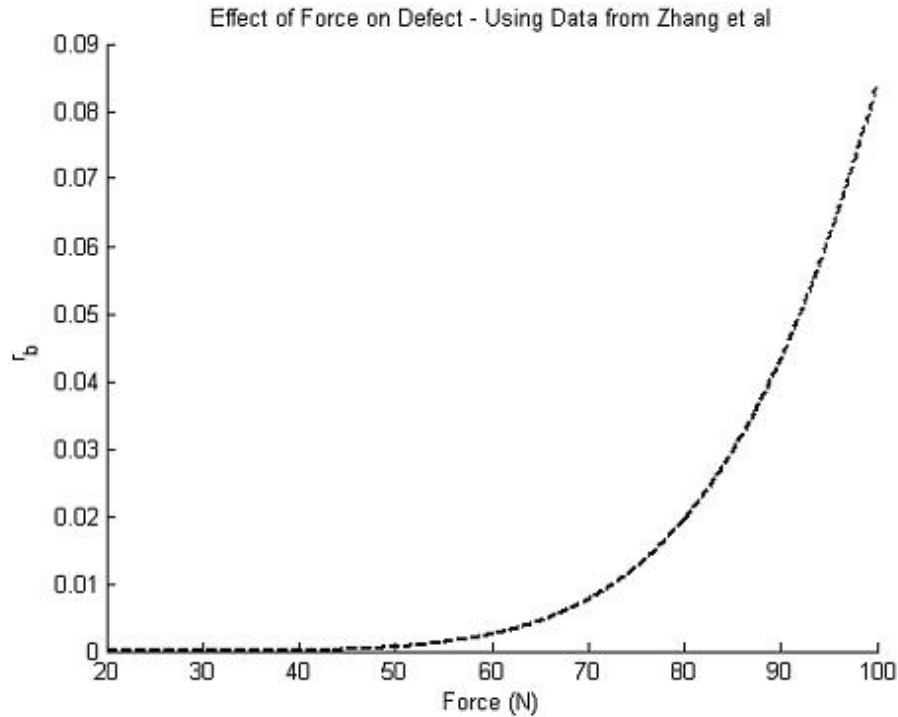
Figure 3.10: Defect varying with thrust force applied to data from Zhang et al [32]

zone varies as a function of thrust force. More importantly, with increasing thrust force, the edge defect does not start to become flat, but continues to increase. This is because the delaminated zone increases with increasing thrust force, and a larger delamination zone results in a greater length of fiber bending and hence a larger defect.

3.5   Experimental Comparisons

Based on studying drilled CFRP samples, it is apparent that it is difficult to accurately measure the size of the defect around a drilled hole. This is because defects are not uniform as the model predicts it to be. Actual defects around a drilled hole include phenomenon such as fiber pull-out which can be very difficult to model. During measurement, it is also difficult to differentiate between fibers of different lamina. Due to this, the uncut-fibers around the hole cannot be attributed solely to the phenomenon the model is trying to capture. Thus, quantitative measurements are not very accurate and a qualitative assessment of the model is performed.

The model predicts an elliptical defect profile around the hole, which was seen in Figure

3.5. Also, the model predicts that the size of the defect increases with increasing feed. This can be seen in Figures 3.11 and 3.12, which are respectively two cases of drilling through HM-CFRP material at low (.1mm/rev) and high (1mm/rev) feeds respectively.

Figure 3.11: Defect during low-feed drilling

Figure 3.12: Defect during high-feed drilling

The experimental observations also show that there is significant downward bending of the uncut fibers due to the drill feed. Hence, the defects are out of the cutting plane which may also cause debris accumulation and improper mating during assembly.

3.6 Techniques to Quantify Edge Defects in FRP Machining

Measuring the defects around a hole edge during FRP machining is challenging due to several reasons, including the out-of-plane nature of the defects and because the brittle fibers break during measurement. Also, sometimes the defects themselves may not be of concern, but the debris they cause during assembly may be an issue. It is again instructive to draw comparisons between FRP drilling and metal drilling to better understand techniques for quantitative characterization as metrology and process control methods for metal machining are more advanced.

Non-contact optical techniques have been successfully demonstrated to measure edge-defects formed during micro-drilling [38]. Since these methods do not rely on the properties of the material being machining, they are ideal for application in the case of FRPs. Ko and Park [38] demonstrated that the Conoscopic Holography method is best suited as it can capture very small features, which is very important in the case of FRPs as the fibers can be only a few-hundred microns in diameter. It is also possible to use the Conoscopic method to obtain 3D profiles of the burr. This information, along with the mechanical properties of the fibers can be used to estimate the behavior of the edge defects during assembly.

Inductive probes have also been very successfully used to measure burrs during metal drilling [39]. These probes are small and can be easily be integrated into the process flow to provide in-situ monitoring of the process quality. While inductive sensors themselves are not applicable for FRPs as FRPs do not respond to a magnetic field, a similar approach of using sensors integrated into the manufacturing process will be useful.

Ultimately, a standardized method to formally characterize the tolerable defect around an edge is needed for optimal manufacturing with minimal waste of effort from over-precision. Several characterization methods have been used for metal burrs ([40, 41]) and these can be adapted and extended to include FRP machining as well.

3.7 Future Work

Future work includes reformulating the model by taking non-linear effects into consideration. This will necessitate revisiting the derivation of the critical thrust force for delamination and including factors such as material and geometric non-linearity, as well as transverse shear deformation which is an important effect in laminated polymer composites. With a non-linear approach, it will also be possible to arrive at an analytical estimate of the size of the

delaminated zone. Also, using some of the measurement techniques outlined, experimental tests have to be employed to assess the accuracy of the model. More sophisticated models can also take into account cutting dynamics; however, given the complexity of the drill geometry and the different phases in the workpiece, these models will need numerical modeling approaches to arrive at practical solutions to this complex problem.

Chapter 4

Automated Drill Design Software

This section discusses the development of an automated drill modeling tool in Solidworks. The tool uses Solidworks to generate a 3D model of a drill based on manufacturing parameters of the drill supplied by the user. The need to use manufacturing parameters to model drills will be established. The applet uses a GUI to accept these parameters from the user and generates the model "on-the-fly". The applet allows the user to save the model in a variety of formats which can be them imported into a meshing program or into the meshing module of an FEA package for subsequent use in FE-based simulations. The applet was written using Visual Basic APIs in SolidWorks 2003 and is forward-compatible with SolidWorks 2005. The current version of the applet is restricted to designing two-flute twist drills.

The subsequent sections discuss geometry of conventional two-flute drills and how they are designed and manufactured. This is followed by a discussion of the 3D analytical formulation of drill geometry. After this, an algorithm to model drills using commercial CAD tools is discussed. Finally, the report presents implementing this algorithm in Solidworks to create an automatic drill geometry modeling tool.

4.1 Design and Manufacturing of Drills

4.1.1 Description of Drill Geometry

The geometry of two-flute twist drills is shown in Figure 4.1. For more information on the standard description of features and geometry of drills, the reader is referred to Galloway [42] and the ASM Handbooks
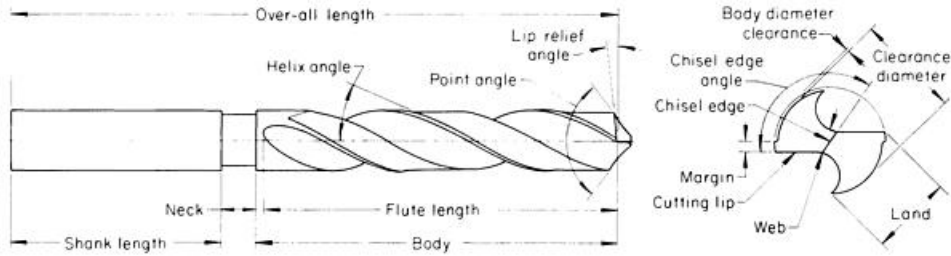[43].

Figure 4.1: Standard Geometry of Two-Flute Twist Drill [43]

4.1.2 Manufacturing - Two-Flute Drills

The geometric parameters of conventional two-flute twist drills are determined by its manu-facturing parameters. Drill manufacturing consists primarily of two grinding steps, namely grinding the flute faces and grinding the flank faces. The parameters of these grinding op-erations determines the geometric parameters of the drill. Parameters such as point angle and web thickness are implicit functions of the drill's manufacturing parameters.

Let us first take a look at how a two-flute twist drill is manufactured. The starting material is a cylindrical rod (or bar-stock) that is the of same diameter as required in the drill. During flute grinding (see Figure 4.2), the grinding wheel rotates in-place with the drill simultaneously rotating about and moving down its axis. The dual motion of the drill controls the helix angle of the flute and the position and profile of the grinding wheel controls the cross-section of the drill flute. In a two-flute drill, this is performed twice at orthogonal positions to generate both flutes.

Figure 4.2: Flute Grinding [44]

During flank grinding, the grinding wheel rotates about a fixed axis to form a "grinding cone" of cone-angle θ (see Figure 4.3) and the dill rotates "in-place". This grinding is also performed twice from symmetric positions to generate both flank surfaces. These flank surfaces can be considered as sections of the grinding cones.

Figure 4.3 also shows some of the control parameters during flank grinding. The coor-dinate system of the grinding cone is rotated angle ϕ CCW in the $x - z$ plane with respect to the drill's coordinate system. The grinding cone's vertex is located a fixed distance d
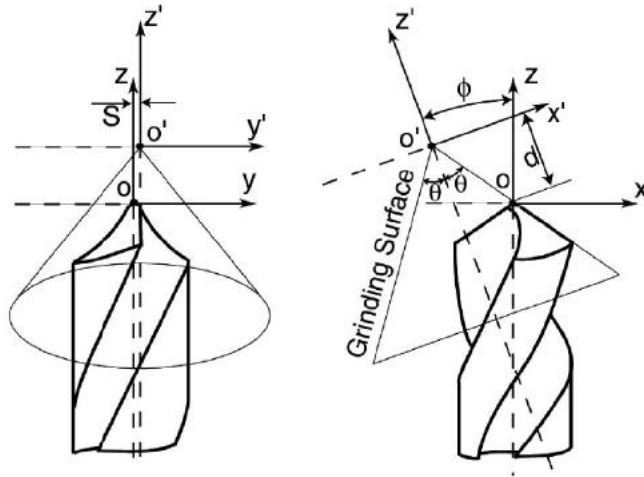
31

Figure 4.3: Flank Grinding [45]

from the tip of the drill, as measured along this rotated coordinate system. Finally, the vertex is shifted a distance S in the y axis. The figure shows the position of a grinding cone that will generate the right-flank surface of a drill. A similar grinding cone is symmetrically positioned to grind the right cone surface.

The next section will discuss how the manufacturing parameters such as grinding wheel cross-section and axis of rotation determine the geometric parameters of the drill. We will also see that the same design features can be generated with multiple sets of manufacturing parameters. Before we take a look at an analytical formulation of the drill geometry, past work in characterizing the drill geometry - based on which much of the work in this report has been developed - is discussed.

4.2 Literature Review

Galloway [42] initiated a formal study of drill geometry in his seminal ASME paper where he discussed several aspects of the drilling process. Subsequent researchers built on his basic framework and extended his analytical equations to develop computer-based models. Fujii et al [46, 47] developed algorithms to develop drill models using a computer. The drill geometry was analyzed by considering the "slicing" of the drill by arbitrary planes. A computer model was also developed to design a twist drill. Tsai and Wu [48] also presented explicit mathematical equations to describe the drill point geometry. These equations covered the conventional conical drills as well as the ellipsoidal and hyperboloidal drills. The effect

of grinding parameters on various cutting angles was also discussed.

As regards to developing meshed drills for FE-applications, Hsu [18] performed the first FEM simulations for drilling. He developed a drill-mesher that produced a mesh of a two-flute twist drill based on user supplied parameters. The drill was designed using similar manufacturing-based techniques as discussed in the previous section. The mesher could output a surface mesh as well as a hexahedral volume mesh in different formats for use in various packages. Choi [17] used analytically defined flank sections and twisted them down a helical path to fully define the drill geometry. He developed an applet to generate a 3D FE-mesh based on this technique for processing in Abaqus. This applet was capable of generating n-flute geometry.

4.3 Overview of Modeling Procedure

Existing drill design methods rely extensively on discretized analytical equations. Errors and approximations from the discretization can affect the quality of the final drill design. A modeling technique that closely mimics the manufacturing process will be of use here as this will offer the maximum reduction of discretization errors. Also, as solid modeling software get more powerful, it make sense to use the powerful geometric modeling capabilities of these packages instead on relying on manually written equations and algorithms. Also, as we would like use these drill models in various different FEM packages, its cumbersome to generate meshes specific to each package. As modern software packages can import open-source standard solid models (eg., ACIS-SAT, STL), it is very convenient to design the drill using standard CAD techniques so that it is in a format that can be converted/viewed in a variety of platforms.

The drill modeling procedure discussed in this report tries to address these issues, and provides an easy way to generate arbitrary two-flute drill geometry using commercial CAD packages in a portable format. The modeling algorithm mimics the manufacturing process by performing boolean subtraction operations corresponding to the grinding steps preserving the order in which these steps are performed. The following section discusses the analytical formulation of the model upon which the algorithm is developed.

4.4 Analytical Formulation

4.4.1 Basics

It is useful to first define a coordinate system that will serve through the analysis. The same coordinate system from previous studies [46, 47, 48] is used to allow easy comparison. The axes of the system, x, y, z, are described as follows:

- x-axis - Parallel to the secondary cutting edge of the drill flank

- z-axis - Parallel to the axis of the drill

- y-axis - Orthogonal to the x and z axes

4.4.2 Flute Shape

The cross-section the flute is dependent on the shape of the grinding wheel used for grinding it. The cross-section of the drill has to be designed such that it generates a straight secondary cutting edge when the flanks are ground. Hence, the shape of the flute grinding wheel is dependent on the specifications of the drill that is being ground. Instead of describing the grinding wheels, we can directly consider the cross sectional profile of the flute. The cross-section of the flute can be divided into 8 sections as shown in Figure 4.4. Sections 1, 2, 3, 4 are unground parts of the drill-blank and are arcs which make up a circle. Sections 5 and 6 can be described by the following polar equation:

$$\psi = \sin^{-1}\frac{W}{2r} + \frac{\sqrt{r^2 - \left(\frac{W}{2}\right)^2}}{r}\tan h \cot p$$

where, W is the web thickness, r is the radius of the drill, h is the helix angle and p is the half-point angle.

Here, r is varied from $\frac{W}{2}$ to R. This polar equation makes sure that the flank section produces a drill with a straight cutting edge. Sections 7 and 8 do not contribute much to the cutting performance of the drill and only need to be optimized to provide rigidity. For simplicity, they can be modeled as symmetric to sections 5 and 6 respectively.

To convert the flute profile from 2D to a 3D boundary surface, a z-component term can be appended to the equation to capture the helical profile. The z-component term is as follows (for a drill of radius r:
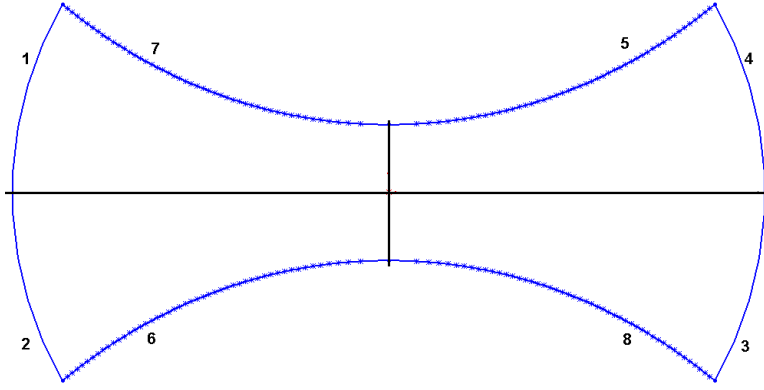
$$z_{flute} = \frac{tanh}{r}z$$

34

Figure 4.4: Flute Cross-Section

Here, h is the peripheral helix angle, and is (for a drill of length l):

$$h = tan^{-1}\frac{2\pi r}{l}$$

4.4.3 Flank Shape

Figure 4.3 showed the coordinate system of the grinding cone. Let us define the axes of this system as $\{x^*, y^*, z^*\}$. The relationship between this coordinate system and the drill's coordinate system $\{x, y, z\}$ is given as follows:

$$\begin{bmatrix} 1 \\ x^* \\ y^* \\ z^* \end{bmatrix} = T \begin{bmatrix} 1 \\ x \\ y \\ z \end{bmatrix} \tag{4.1}$$

where, T is the transformation matrix:

$$T = \begin{bmatrix} 1 & 0 & 0 & 0 \\ -\sqrt{d^2 \tan^2 \theta - S^2} & \cos \phi & 0 & \sin \phi \\ -S & 0 & 1 & 0 \\ d & -\sin \phi & 0 & \cos \phi \end{bmatrix} \tag{4.2}$$

From the figure, we can see that the cone vertices are defined at $(0, 0, 0)$ of the cone-

coordinate system. This position in the drill coordinate system is given by:

$$
\begin{bmatrix} 1 \\ x_v \\ y_v \\ z_v \end{bmatrix} = T^{-1} \begin{bmatrix} 1 \\ 0 \\ 0 \\ 0 \end{bmatrix}
\tag{4.3}
$$

Thus, the vertices of the grinding cone are as follows:

Right Cone:

$$
x_v = -(\sqrt{d^2 \tan^2 \theta - S^2} \cos \phi + d \sin \phi)
$$

$$
y_v = S
$$

$$
z_v = d \cos \phi - \sqrt{d^2 \tan^2 \theta - S^2} \sin \phi
$$

Left Cone:

$$
x_v = \sqrt{d^2 \tan^2 \theta - S^2} \cos \phi + d \sin \phi
$$

$$
y_v = -S
$$

$$
z_v = d \cos \phi - \sqrt{d^2 \tan^2 \theta - S^2} \sin \phi
$$

4.4.4 Required Parameters

From the above analysis, we can see that the following parameters (geometric and manufacturing) are needed to completely describe a drill:

Geometric -

R	Radius of drill
w	Web thickness
h	Helix angle
p	Half-point angle

Manufacturing -

d	x-shift of cone (in cone-coordinate system)
S	y-shift of cone (in cone-coordinate system)
θ	Cone angle

It may make more intuitive sense to describe a drill using additional geometric parameters such as the relief angle or the chisel edge angle (and not the manufacturing parameters),

but the objective of this report is to present a modeling algorithm that closely follows the manufacturing process. Hence, the algorithm uses these (non-intuitive) manufacturing parameters instead of the additional geometric parameters. In most cases, when a drill is specified, it is descirbed using these additional geometric parameters. But these parameters are implicit functions of the parameters discussed above. For example, the chisel edge angle (ξ) is expressed as:

$$\xi = \pi - \tan^{-1}\left(\frac{\sqrt{\tan^2\theta d^2 - S^2}\cos\phi - \tan^2\theta d\sin\phi}{S}\right) \tag{4.4}$$

Hence we can see that for a given chisel edge angle, there are multiple sets of possible manufacturing parameters.

4.5   Algorithm Development

Based on the above analytical formulation, an algorithm is presented in this section to realize the drill in a given CAD program. The actual implementation of the algorithm is dependent on the specific features of the individual CAD program in which it is applied.

The general algorithm to develop the geometry of the drill is as follows:

1. Obtain the geometric and manufacturing parameters from the user. Calculate the derived variables from these parameters.

2. Draw the cross-section of the flute and create the solid flute by helical-extrusion

3. Locate the cone vertices

4. Draw the cone axes at these vertices and create a "virtual" cone

5. Use the cones to perform a boolean-subtract cut to generate the flank surfaces of the drill

6. Draw the cross-sections of the drill margin

7. Use helical-extrusion to create the 3D margin volume

8. Perform a boolean-cut operation to remove margin volume

4.6 Algorithm Implementation using Solidworks APIs

4.6.1 Solidworks

Solidworks is a popular 3D modeling CAD package. Solidworks uses a feature-based parametric approach for 3D drawings. Features are defined to create volume and modifications to sketches and these features can be rolled-back or modified to create multiple configurations of the same part. The program uses a feature hierarchy to determine "child" and "parent" features. Solidworks allows models to be saved in many different graphical formats and is hence very useful in ensuring that the model is portable.

Solidworks is also integrated with an API (Application Programming Interface) which contains many functions that can be called from programming languages such as Visual Basic and C++. These functions provide access to Solidworks' graphical engine and can be used to create solid models. Programs can also be written in these programming languages that can accept input to generate user-defined solid models.

4.6.2 Applying Algorithm to Solidworks

The algorithm is applied in SolidWorks as follows.

Coordinate Axis

The same coordinate axis as the analytical formulation is retained in SolidWorks for easy portability.
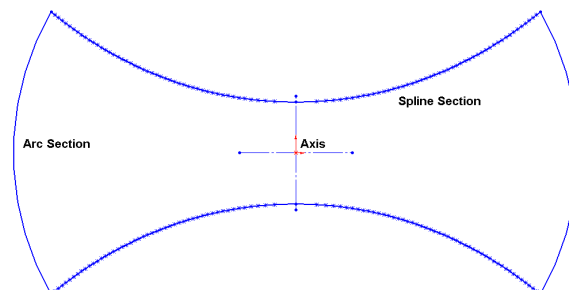
Flute Cross Section

Figure 4.5: Flute Cross Section

As descried earlier, the flute cross-section is symmetric about both the x and the y axes. Hence, it suffices to just draw one quadrant of the flute and mirror it about both axes.

The arc part of the quadrant (Figure 4.5) is generated with the `CreateArcVB` function. A set of points are then generated using the polar function to describe the other part of the cross-section in the quadrant. To create the curve, these points can either be connected with lines or by drawing an interpolated spline function though them. A spline function is more efficient as fewer points need to be sampled to generate a high-quality "fit". Significant performance improvement was noticed when a spline-fit was used instead of a line-fit. The spline was created using the `SketchSpline` function. After one quadrant is completely sketched, "mirror" lines were drawn to denote the X and Y axes using the `CreateLine2` function with the `ConstructionGeometry` option set to `True`. Using these mirror lines, the quadrant was mirrored about both axes and the full flute-cross section was realized. SolidWorks automatically connects the spline functions when they are mirrored to ensure that the profile is closed sketch.
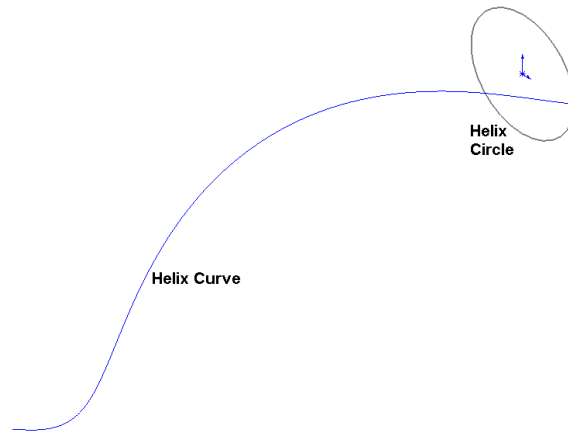
Creating the Solid Flute Body

Figure 4.6: Helix Circle and Helix

To create the solid flute body, the 2D section is swept-extruded about a helical path. In order to define the helical path, a circle denoting the diameter of the helix is first needed. A circle centered at $X = 0, Y = 0$ is generated with the same radius as that of the drill flute using the `CreateCircle` function. The `InsertHelix` command is then used to create the 3D helix using height and number of helical revolutions as parameters. The helix height is the same as the length of the drill flute, and for one revolution this can be calculated based on the drill radius (R) and the helix angle (h) as:

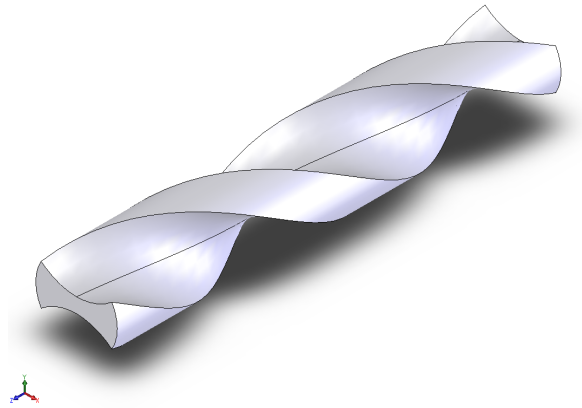$$l_{flute} = \frac{2\pi R}{\tan h} \tag{4.5}$$

Figure 4.7: Solid Flute Body

The sweep-extrusion is performed using the `Part.Extension` routine and this generates the solid flute body.

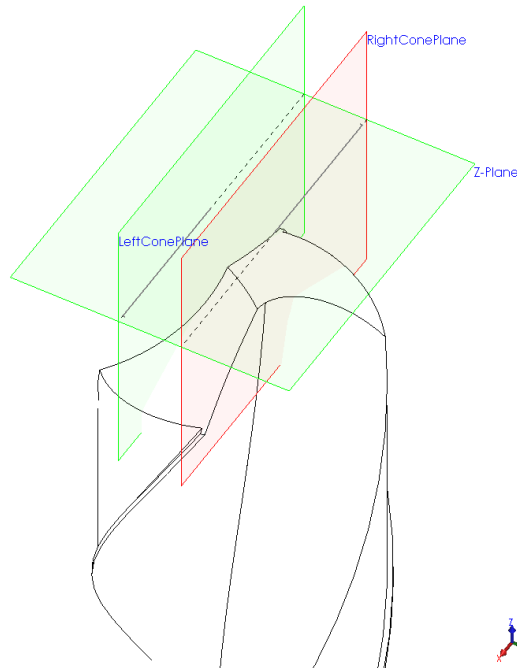**Generating the Flank Surfaces**

Figure 4.8: Planes to Generate Flank Surfaces

The flanks are generated by taking a swept-cut of a conical section around a specifically defined axis. From the analytical formulation, we know that the grinding cone's axis is located on a plane parallel to the $x - z$ plane. Two separate planes have to be defined as we

are considering two flank grinding operations and hence two grinding cones. We also know that the vertex of both grinding cones is located in a plane parallel to the $x - y$ plane. As we know the offset distance, the plane `Z-Plane` is created using the `CreatePlaneAtOffset3` function. Using straight lines drawn on this plane, the orthogonal planes parallel to the $x - z$ planes can be defined (using a line and a plane an orthogonal plane can be defined). The two planes are created using the `CreatePlaneAtAngle3` function.
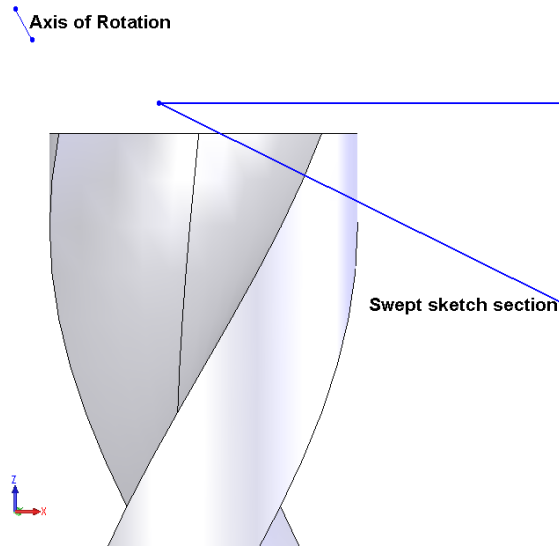

Figure 4.9: Sketch to Cut the Flank

Following this, the cone axis and cone profile are sketched on these planes and a swept-cut is taken. SolidWorks' swept-cut operation works by first generating a volume by sweeping a 2D cross-section about an axis. A boolean operation is then performed and the intersection regions between the swept volume and the volume of a given solid object in the design space is removed from the solid object. In the grinding operation, the cone removes all the material from the drill outside of the cone. Hence the cone profile sketch is designed such that it effectively removes material outside the grinding cone.

This operation is performed twice, once for each set of cone grinding axes and the solid drill geometry is realized after this step.

Drill Margin and Relief

Existing literature does not extensively cover the modeling of the drill margin and relief, hence these features are only approximately drawn. In order to generate these features, we need to know the margin length and the relief width. Using this, a 2D cross-section is
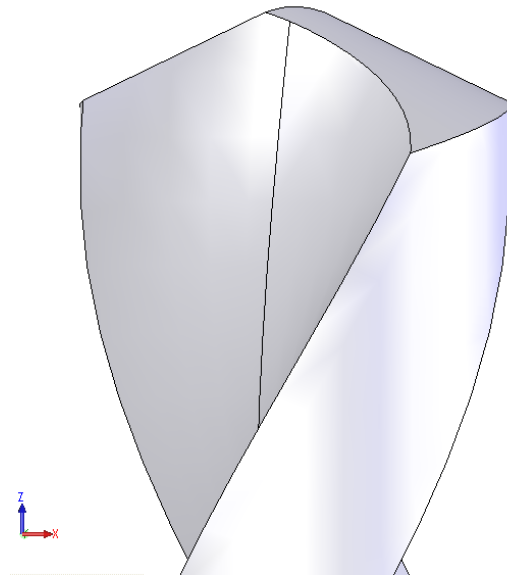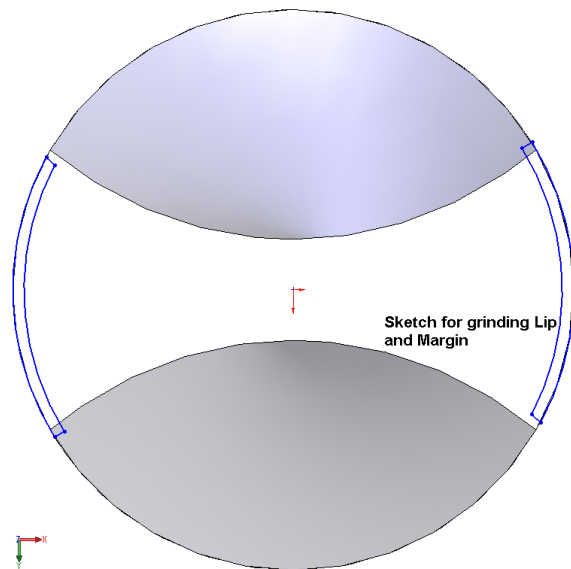
41

Figure 4.10: Solid Drill with both Flanks cut

Figure 4.11: Drawing the Cross-section of the Margin and Lip Relief Cut

drawn on the same plane where the flute was generated, as shown in Figure 4.11 . The same helix which was used to generate the flute is redrawn and the profile is swept-extruded along this helical path. A boolean cut is performed and the 3D volume described by the swept-extrusion is removed from the solid body of the drill.
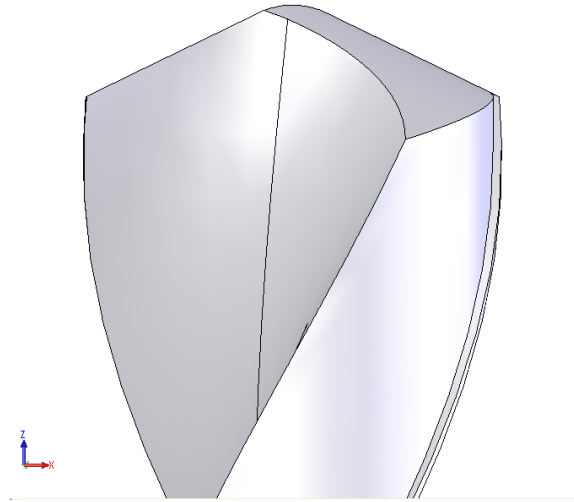

Figure 4.12: Fully Designed Drill

4.7 User Interface Development

Visual Basics APIs was used to design an ergonomic and accessible user interface. The interface accepts inputs from the user regarding the geometric and manufacturing specifications of the drill in SI units. A schematic of a drill with all the dimensions marked is also shown alongside for ease-of-use. After entering the data, the user can click the "Generate Drill" in order to invoke the necessary Solidworks commands to execute the program. Following a brief wait, the drill is generated in Solidworks. The user now has the option of saving the drill in a variety of formats, which can then be imported into either a Finite Element program for subsequent analysis. Currently, the software supports saving the drill in the .SLDPRT (Solidworks), .SAT (ACIS) and .IGS (International Graphics Exchange) formats. The user interface is shown in Figure 4.13.
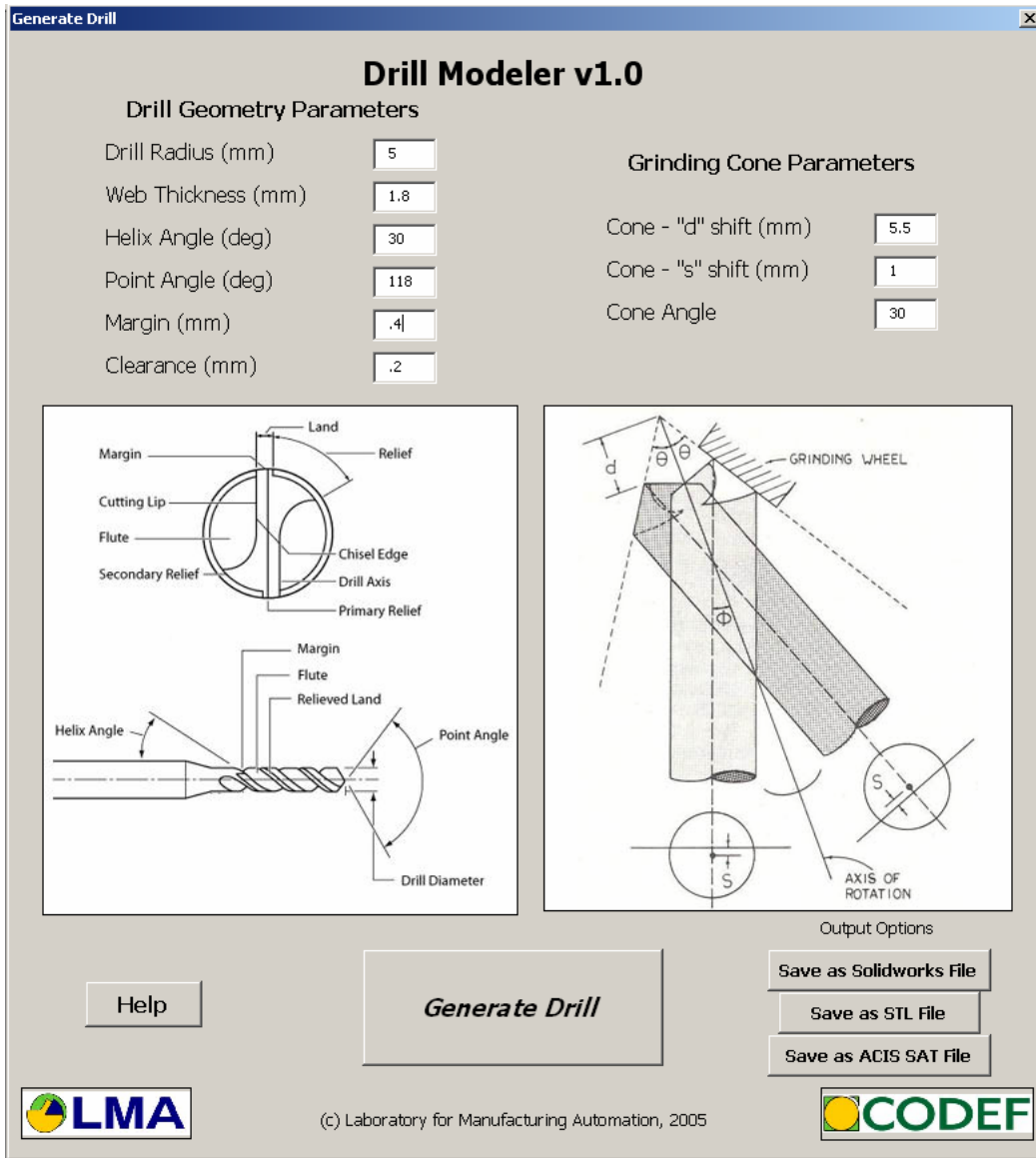
Figure 4.13: Drill Modeler, GUI

4.8   Results

Using the capability of the software to save in different formats, a drill was generated and exported into Abaqus and DEFORM using the SAT and STL formats, respectively. The drills were then meshed using the meshing module of these two packages. The resultant meshes along with the original solid model can be seen in Figure 4.14.

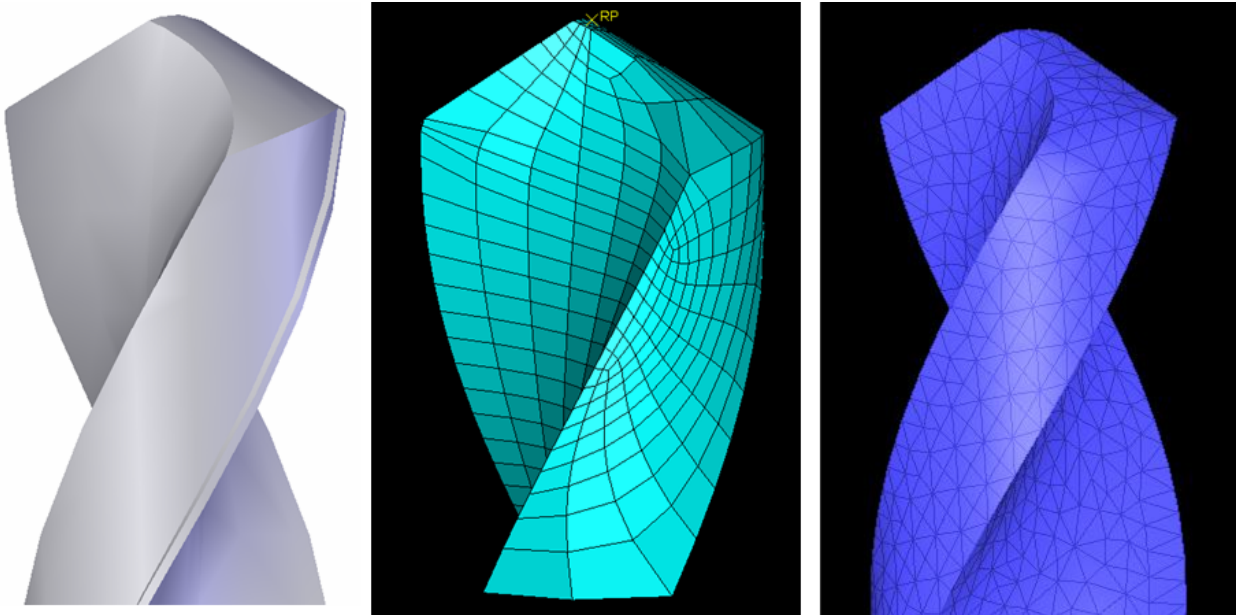Figure 4.14: Solid Model (left), Meshed in Abaqus (middle), and Meshed in DEFORM (right).

4.9   Future Work

Future work includes expanding the package to model different drill types. A module that permits the description of arbitrary ground geometries can also be included. Physical prototypes of the drill also have to be created and compared with regular drills to validate the accuracy of the modeling technique.

Chapter 5

Conclusions

As mentioned earlier in the Introduction, although these two projects seem unrelated, they contribute to solving the larger problem of developing a fully featured numerical model of FRP machining. The defect prediction model is a simple first-order relationship which relates defects observed during FRP drilling to material properties and process parameters. The model shows good qualitative agreement with experimental results. The model establishes high thrust forces as the main cause for these defects. Using new drills which demonstrate lower thrust forces, and using pre-machining techniques such as pilot holes will reduce the delamination and thus the occurrence of these defects. Again, the importance of using models that relate material properties to machining phenomenon cannot be overstated. This is especially true in the case of composite materials such as FRPs which tend to have a large range of material properties. It will be impossible to empirically model the machining of all the FRP materials that are being used, and only a fundamental understanding of material properties will lead to sustainable improvements in the efficiency of the machining process.

The other project presented - the drill modeling tool - is a quick way to generate accurate models of twist drills. Drill models from this tool have been successfully applied in Finite Element simulations in two different software packages, Abaqus and DEFORM. The tool demonstrates that using advanced CAD packages it is possible to mimic the material-removal of a grinding operation and thus create very accurate models of ground parts. Grinding operations can be abstracted to a boolean subtract operation using a revolved cut, with the grinding wheel profile and axis of revolution as input parameters. Using this general design methodology, more complex drill models can also be abstracted to a series of grinding operations and thier solid models can be easily created.

The software code used in this project is available online at:

<div align="center">http://me.berkeley.edu/~athulan/masters/</div>

Bibliography

[1] Callister, W., 1999. *Materials Science and Engineering: An Introduction.* John Wiley and Sons Inc., New York.

[2] of Virginia, U., 2005. Me 257 - composite materials. http://www.emba.uvm.edu/ iatridis/me257/Introduction.htm.

[3] Reddy, J. N., 2003. *Mechanics of Laminated Composite Plates and Shells.* CRC Press.

[4] Ffield, P., 2005. Personal communication. Boeing Corp, Seattle, WA.

[5] S.A.S, A., 2005. Airbus a380. http://www.airbus.com.

[6] Boeing, 2005. Boeing commercial airplanes - 787. http://www.boeing.com.

[7] of Competence, F. M. L. C., 2005. Glare. http://www.fmlc.nl.

[8] Shaw, M. C., 2005. *Metal Cutting Principles.* Oxford University Press.

[9] Trent, E. M., and Wright, P. K., 2000. *Metal Cutting.* Butterworth-Heinenmann.

[10] Komvopoulos, K., and Erpenbeck, S. A., 1991. "Finite element modeling of orthogonal metal cutting". *Journal of Engineering for Industry,* **113**, pp. 253–267.

[11] Strenkowski, J. S., and Carroll, J. T., 1985. "A finite element model of orthogonal metal cutting". *Journal of Engineering for Industry,* **107**, p. 349354.

[12] Huang, J. M., and Black, J. T., 1996. "An evaluation of chip separation criteria for the fem simulation of machining". *Journal Of Manufacturing Science and Engineering,* **118**, pp. 545–554.

[13] Ortiz, M., and Marusich, T. D., 1995. "Modelling and simulation of high-speed machining". *International Journal for Numerical Methods in Engineering,* **38**, pp. 3675–3694.

[14] Klocke, F., Raedt, H.-W., and Hoppe, S., 2001. "2d-fem simulation of the orthogonal high speed cutting process". *Machining Science and Technology,* **5**(3), pp. 323–340.

[15] Park, B., 1996. "Modeling of burr formation processes in metal cutting". PhD thesis, University of California, Berkeley.

[16] Min, S., Dornfeld, D., Kim, J., and Shyu, B., 2001. "Finite element modeling of burr formation in metal cutting". *Machining Science and Technology,* **5**(2), pp. 307–322.

[17] Choi, J., Min, S., Dornfeld, D. A., Alam, M., and Tzong, T., 2003. "Modeling of inter-layer gap formation in drilling of a multilayered material". In CIRP International workshop on modeling of machining operations.

[18] Hsu, B., 2002. "Computer simulations for burr formation study". PhD thesis, University of California, Berkeley.

[19] Weinert, K., and Kempmann, C., 2004. "Cutting temperatures and their effect on the machining behaviour in drilling reinforced plastic composites". *Advanced Engineering Materials,* **6**(8), pp. 684–689.

[20] Matthews, F. L., Davies, G. A. O., Hitchings, D., and Soutis, C., 2000. *Finite Element Modeling of Composite Materials.* Woodhead Publishing Limited.

[21] Soden, P. D., Hinton, M. J., and Kaddour, A. S., 1998. "A comparison of the predictive capabilities of current failure theories for composite laminates". *Composites Science and Technology,* **58**, pp. 1225–1254.

[22] Hinton, M. J., Kaddour, A. S., and Soden, P. D., 2002. "A comparison of the predictive capabilities of current failure theories for composite laminates, judged against experimental evidence". *Composites Science and Technology,* **62**, p. 17251797.

[23] Komanduri, R., 1995. "Machining fiber-reinforced composites". *Mechanical Engineering,* **115**, pp. 58–64.

[24] Bhatnagar, N., Ramakrishnan, N., Naik, N. K., and Komanduri, R., 1995. "On the machining of fiber reinforced plastic (frp) composite laminates". *International Journal of Machine Tools and Manufacturing,* **35**, pp. 701–716.

[25] Gordon, S., and Hillery, M. T., 2003. "A review of the cutting of composite materials". In Proceedings of the Institution of Mechanical Engineers, Vol. 217, pp. 35–45.

[26] Arola, D., Sultan, M. B., and Ramulu, M., 1999. "A finite element analysis of chip formation in the machining of fiber reinforced plastics". *Transactions of NAMRI,* **27**, pp. 93–98.

[27] Mahdi, M., and Zhang, L., 2001. "An adaptive three-dimensional finite element algorithm for the orthogonal cutting of composite materials". *Journal of Material Processing Technology,* **113**, pp. 368–372.

[28] Mahdi, M., and Zhang, L., 2001. "A finite element model for the orthogonal cutting of fiber-reinforced composite materials". *Journal of Material Processing Technology,* **113**, pp. 373–377.

[29] Hocheng, H., and Dharan, C. K. H., 1990. "Delamination during drilling in composite laminates". *Journal of Engineering for Industry,* **112**, pp. 236–239.

[30] Jain, S., and Yang, D. C. H., 1994. "Delamination-free drilling of composite laminates". *Journal of Engineering for Industry,* **116**, pp. 475–481.

[31] Lachaud, F., Piquet, R., Collombet, F., and Surcin, L., 2001. "Drilling of composite structures". *Composite Structures,* **52**, pp. 511–516.

[32] Zhang, H., Chen, W., Chen, D., and Zhang, L., 2001. "Assessment of the exit defects in carbon fiber-reinforced plastic plates caused by drilling". *Key Engineering Materials,* **196**, pp. 43–52.

[33] Bhatnagar, N., Singh, I., and Nayak, D., 2004. "Damage investigation in drilling of glass fiber reinforced plastic composite laminates". *Materials and Manufacturing Processes,* **19**(6), pp. 995–1007.

[34] Won, M. S., and Dharan, C. K. H., 2002. "Drilling of aramid and carbon fiber polymer composites". *Journal of Manufacturing Science and Engineering,* **124**, pp. 778–783.

[35] Timoshenko, S., and Woinowsky-Kreiger, S., 1959. *Theory of Plates and Shells*, 2nd ed. McGraw Hill, New York.

[36] Shaw, M. C., and Jr, C. J. O., 1957. "On the drilling of metals: Part 2 the torque and thrust in drilling". *Transactions of the ASME,* **79**, pp. 139–148.

[37] Ho-cheng, H., 1988. "An analysis of drilling of composite materials". PhD thesis, University of California, Berkeley.

[38] Ko, S. L., and Park, S. W., 2004. "2004development of effective measurement system for burr geometry". In Proc. of the 7th International Conference on Deburring and Surface Finishing, pp. 173–180.

[39] Jagiella, M., and Fericean, S., 2004. "Inductive sensor system for evaluation of burrs and edges in industrial application". In Proc. of the 7th International Conference on Deburring and Surface Finishing, pp. 89–102.

[40] Gillespie, L. K., 1996. Burr and edge standards: A compilation of standards. Tech. rep., Worldwide Burr Technology Committee.

[41] Berger, K., 2004. "Proposal for a standard for the description of edges in automotive engineering". In Proc. of the 7th International Conference on Deburring and Surface Finishing, pp. 67–80.

[42] Galloway, D. F., 1957. "Some experiments on the influence of various factors on drill performance". *Transactions of ASME,* **79**, pp. 191–231.

[43] Committee, A. I. H., 1999. *ASM Metals Handbook.* ASM International.

[44] USCTI, 1989. *Metal Cutting Tools Handbook*, 7th ed. Industrial Press Inc.

[45] Ren, R., and Ni, J., 1999. "Analyses of drill flute and cutting angles". *Int. Journal of Advanced Manufacturing Technology,* **15**, pp. 546–553.

[46] Fujii, S., DeVries, M. F., and Wu, S. M., 1970. "An analysis of drill geometry for optimum drill design by computer. part i - drill geometry analysis". *Journal of Engineering for Industry,* **92**, pp. 647–656.

[47] Fujii, S., DeVries, M. F., and Wu, S. M., 1970. "An analysis of drill geometry for optimum drill design by computer. part ii - computer aided design". *Journal of Engineering for Industry,* **92**, pp. 657–666.

[48] Tsai, W. D., and Wu, S. M., 1979. "Measurement and control of the drill point grinding process". *International Journal of Machine Tools and Manufacturing,* **19**(1), pp. 109–120.